soil systems

MDPI

Article

A Two-Part Harmony: Changes in Peat Molecular Composition in Two Cores from an Ombrotrophic Peatland (Tremoal do Pedrido, Xistral Mountains, NW Spain)

Antonio Martínez Cortizas [1,2,*], Ainé Francos Golán [3,4], Mohamed Traoré [5] and Olalla López-Costas [3,4,*]

1 CRETUS, EcoPast (GI-1553), Facultade de Bioloxía, Universidade de Santiago de Compostela, 15782 Santiago de Compostela, Spain
2 Bolin Centre for Climate Research, Stockholm University, 106 91 Stockholm, Sweden
3 CRETUS, EcoPast (GI-1553), Area of Archaeology Department of History, Facultade de Xeografía e Historia, Universidade de Santiago de Compostela, 15782 Santiago de Compostela, Spain; aine.francos.golan@usc.es
4 Archaeological Research Laboratory, Wallenberglaboratoriet, Stockholm University, 106 91 Stockholm, Sweden
5 Advanced Materials Department, Fundación Centro Tecnológico de Investigación Multisectorial (CETIM), 15180 Culleredo, Spain; traore.mohamed19@gmail.com
* Correspondence: antonio.martinez.cortizas@usc.es (A.M.C.); olalla.lopez@usc.es (O.L.-C.); Tel.: +34-881813379 (A.M.C.); +34-881816007 (O.L.-C.)

Abstract: In peat research, the question often arises as to how similar/different the records of cores collected in the same mire are. This has been addressed for some metals (e.g., Pb and Hg), but the question remains open for the molecular composition of organic matter (pOM). Here, we explore this issue by analysing two cores from a raised bog, combining FTIR-ATR, mid-infrared (MIR) indices, and principal component analysis (PCA), and support the interpretation with multilinear regression (MLR) modelling of peat physical (colour) and elemental (C, N, and C/N) properties. The MIR indices and principal components showed depth patterns mainly related to long- and short-term peat decomposition, as well as other secondary changes involving some compounds (e.g., lignin). The depth records of the two cores are remarkably similar, indicating they were synchronously affected by the same processes and to almost the same degree. Cellulose crystallinity was the only property that showed differences in intensity. The good-to-excellent fitting of the MLR models supports the usefulness of FTIR-ATR in peat research. Further studies in a larger number of cores, from the same peatland and from different types of peatlands, are needed to better understand the spatio-temporal responses of the pOM and the factors involved.

Keywords: FTIR-ATR; raised bog; peat organic matter

check for updates

Academic Editor: Heike Knicker

Received: 30 December 2024
Revised: 31 January 2025
Accepted: 7 February 2025
Published: 12 February 2025

Citation: Martínez Cortizas, A.; Francos Golán, A.; Traoré, M.; López-Costas, O. A Two-Part Harmony: Changes in Peat Molecular Composition in Two Cores from an Ombrotrophic Peatland (Tremoal do Pedrido, Xistral Mountains, NW Spain). *Soil Syst.* **2025**, *9*, 14. https://doi.org/10.3390/soilsystems9010014

Copyright: © 2025 by the authors. Licensee MDPI, Basel, Switzerland. This article is an open access article distributed under the terms and conditions of the Creative Commons Attribution (CC BY) license (https://creativecommons.org/licenses/by/4.0/).

1. Introduction

Peatlands, which cover only 3% of the Earth's land surface, are key ecosystems in the global carbon cycle, representing nearly one-third of global soil carbon stocks [1–3]. They perform critical ecological functions, helping to mitigate global warming, and act as carbon sinks due to peat accumulation in waterlogged, anaerobic conditions, which promotes their function as climate archives [3]. Additionally, peatlands are well-known natural archives that enclose a detailed record of Earth's climate history based on proxies for environmental conditions associated with plant and animal remains, isotopes, and pollen grains [4–6], as well as record archaeological information, e.g., metal pollution [7–9]. However, human activities such as drainage and peat extraction can disrupt peatlands' ecological functions, affecting their crucial role in biogeochemical cycles, particularly in the carbon cycle [2,10].

Thus, understanding peatland functioning and the impacts of anthropogenic activities is vital for developing effective climate mitigation strategies.

Peat is formed through the slow accumulation of partially decomposed plant material in waterlogged, anaerobic environments typically found in wetlands (e.g., bogs, fens, and swamps). Its composition is primarily organic matter resulting from plant material (e.g., mosses, sedges, and shrubs), which comprises carbohydrates, lignin, and humic substances [11–13]. In addition, part of the peat composition is associated with a relatively low mineral content influenced by factors related to underlying geology [11,12,14]. Its chemistry is shaped by factors such as vegetation type, hydrological conditions, seasonality, and climate, which together determine the preservation of organic compounds and the input of dissolved inorganic solutes [1,2,10,11]. Over the past years, advances in studies of peat's chemical composition have been crucial for understanding various characteristics, including peat type, decomposition processes, forming vegetation, and environmental responses [15–17].

Among the variety of techniques that are employed to investigate peat's chemical composition, infrared spectroscopy (IR) is widely applied for its ability to detect both organic and inorganic components, offering a direct and cost-effective approach [18–20]. More recently, Fourier-transform infrared spectroscopy with attenuated total reflectance (FTIR-ATR) has gained significant attention due to its high accuracy, minimal sample preparation, and the capacity to process large sample sets quickly [20–22]. Combined with multivariate statistical analyses, FTIR-ATR provides valuable insights into peat's chemical variability, though challenges remain in interpreting overlapping vibrational bands [17,19]. Present FTIR research conducted on peatlands is predominantly focused on changes in peat composition and decomposition processes. However, the versatility of FTIR data makes a suitable tool to also study spatial, ecological, hydrological, and microtopographical variations in a single peatland.

Most current studies are based on single cores as representative of total peatland variability in depth, ignoring the fact that responses might vary inside the same peatland. Factors related to the damage caused to peatlands during sampling, the analytical costs, research time, and the complexity of results prevent researchers from exploring the spatial variability in depth inside the same peatland. A few studies have investigated the spatial variation in metal content by analysing multiple short cores (few tens of centimetres) from the same bog (e.g., references [23,24]) or assessing carbon stocks (e.g., references [25,26]), but, to our knowledge, no previous investigations have focused on comparing the molecular composition of the peat on replicate cores despite the many factors that can affect it (e.g., temporal and spatial variations in vegetation communities, peat decomposition, dust accumulation, etc.). Notwithstanding, how peat's chemical composition might vary in depth within a single peatland remains underexplored.

The present study aims to investigate the chemical variability within a single peatland. To achieve this, FTIR-ATR is applied to two peat cores collected from the dome of Tremoal do Pedrido, located in O Xistral (Lugo, Galicia, NW Spain). The cores were already available, and new sampling was not needed for this study, avoiding further damage to the peatland. By examining variability in the depth records, this research seeks to deepen our knowledge on whether chemical composition varies between locations in the peatland and in depth within the peat deposit (i.e., with time), ultimately contributing to a more comprehensive characterization of peatland ecosystems and their ability to record past changes.

2. Materials and Methods

2.1. Location, Sampling, and Sample Preparation

Tremoal do Pedrido (43.450° N, 7.529° W) is an ombrotrophic mire located at an elevation of 695 m a.s.l. in the Serra do Xistral, at approximately 30 km inland from the

northern coast of Galicia (NW Iberian Peninsula), in the Spanish province of Lugo (Figure 1). This mire features the typical morphology of a raised dome surrounded by a lower elevation minerotrophic peat belt [27]. The area where the mire is located is characterized by a mean annual temperature of 9.5 °C and a mean annual precipitation of 1500 mm, with low seasonal variability [28]. Geologically, Tremoal do Pedrido lies on metamorphic rocks, primarily paragneiss and schist. Within a local radius of 1 to 10 km, additional lithological units are present, including two-mica granites to the north and south, quartzites to the west, and granodiorites to the east, creating a complex geological setting [29]. The surface vegetation of the mire is highly diverse, consisting of a wide range of species that vary in distribution between the central dome and the fen lag. The central dome is predominantly characterized by a community of sedges, grasses, and mosses, with a limited presence of heathers. While the fen lag is dominated by grasses, it has a lower abundance of mosses and displays a notable presence of rushes [24,27,29].

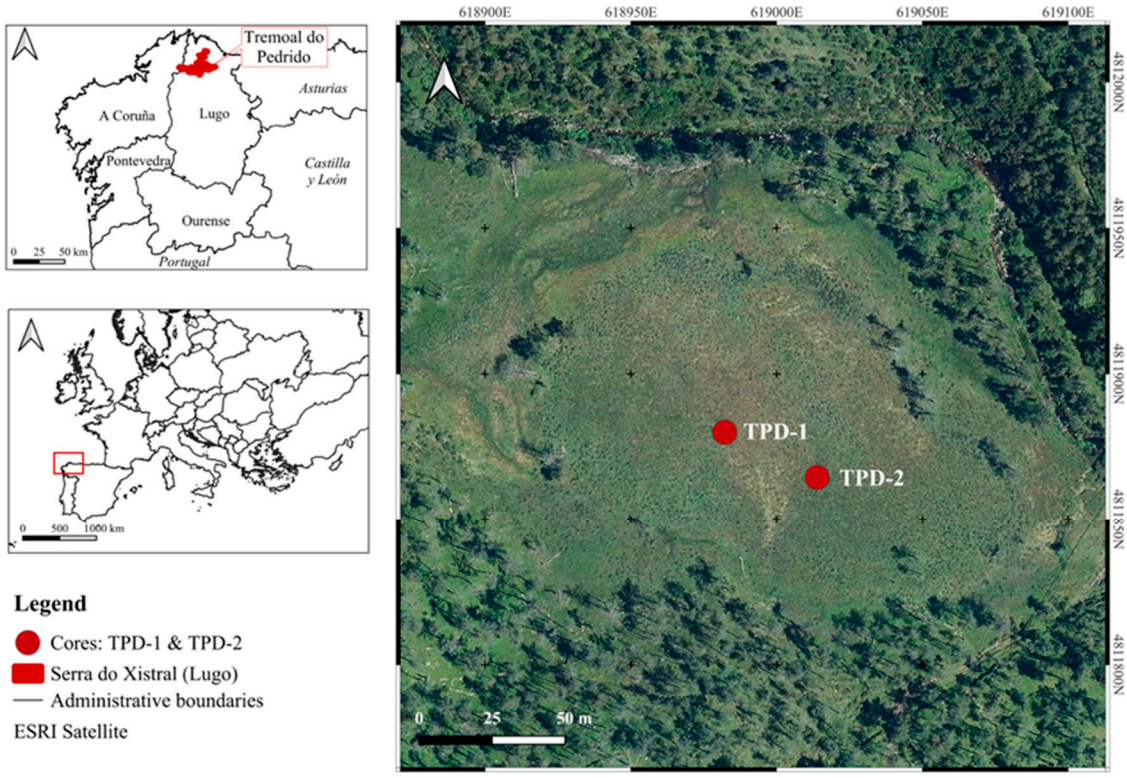

Figure 1. Location map of the Serra do Xistral Mountains (Lugo, Galicia, NW Spain) and the two peat cores collected in the dome of the Tremoal do Pedrido mire.

Two peat cores, designated in the present research as TPD-1 and TPD-2, were collected, at approximately 30 m distance, in 2012 and 2013, respectively. The upper meter of the peat cores was collected using a Waardenar corer of a 10 × 10 cm square section and 110 cm in length; in TPD-1, coring below 1 m was conducted using a Russian peat corer (50 cm long and 10 cm in diameter). TPD-1 was cored to a depth of ca. 4 m for an investigation on atmospheric dust deposition [29], while TPD-2 was sampled to a depth of ca. 1 m for an investigation on microbial carbon consumption [27]. The cores were immediately wrapped in plastic film to preserve their integrity, protected in PVC hemi-tubes, and transported to the laboratory. The cores were sliced into 1 cm sections using a stainless-steel knife, dried at 35 °C, and subsequently milled to achieve homogenization using a Retsch mixer mill MM301 (Retsch GmbH, Haan, Germany) before further analysis. For this study, since

the TPD-2 core is only 1 m deep, we also used the upper meter of the TPD-1 core for comparison, as they were both sampled with the same technique.

2.2. FTIR-ATR Analysis

Fourier-transform infrared spectroscopy with attenuated total reflectance (FTIR-ATR) was employed to analyse a total of 205 samples (105 from TPD-1 and 100 from TPD-2) in the mid-infrared (MIR) region using a Cary 630 spectrometer (Agilent Technologies Inc., Santa Clara, CA, USA) hosted at the EcoPast research group laboratory of the Universidade de Santiago de Compostela. Spectra were recorded within the wavenumber range of 4000–400 cm^{-1} with a resolution of 4 cm^{-1} and an average of 100 scans per sample to enhance the signal-to-noise ratio and ensure data reproducibility. Baseline correction was performed using Orange Data Mining (version 3.38.0; [30]) to avoid bias in the spectroscopic signal due to scattering, reflection, temperature, concentration, or instrument anomalies [31].

2.3. Data Analysis

The first step in the data analysis was to calculate the average, standard deviation, and second-derivative spectra (also using Orange Data Mining) for each of the studied peat cores. This aimed to provide a general description of the spectra, identify the most important absorption peaks, and determine visual differences between TPD-1 and TPD-2. Furthermore, twelve MIR indices commonly used in the literature (Table 1) were calculated and used to determine relative changes in functional groups/peat compounds in relation to the depth/age of the peat samples. In fact, these MIR ratios aim at assessing changes in the molecular structure of the studied peat cores. Some of these indices (LG/PS and CCr) are commonly used to assess changes in the molecular composition of wood and, to our knowledge, are used here for the first time to research peat organic matter composition.

Table 1. Infrared indices used for data analysis.

ID	MIR Ratios (cm^{-1})	Explanation and Indication	References
PS/AL	1030/2920	Polysaccharides/Aliphatics: indicator of the degree of peat decomposition	[32–34]
PS/AR	1030/1600	Polysaccharides/Aromatic: indicator of the degree of peat decomposition	
CB/AR	(1705 + 1730)/1600	Carboxyl/Aromatics: indicator of the relative abundance of carbonyl-rich compounds versus aromatic groups	[32,35]
CCr-1	1370/2920	Crystallinity indices: indicators of the degree of crystalline structure in the molecular structure of cellulose	[36–39]
CCr-2	1425/895		
AL/AR	(2960 + 2920 + 2870 + 2850)/1600	Aliphatics/Aromatics: indicator of alphaticity versus aromaticity	[35]
G/S-1	1265/1311	Guaiacyl/Syringyl lignin: indicators of the evolution of lignin (guaiacyl and syringyl moieties)	[40–43]
G/S-2	1265/1230		
G/S-3	1505/1590		
LG/PS-1	1505/1730	Lignin/Polysaccharides: indicators of relative abundance of lignin versus polysaccharides	[44,45]
LG/PS-2	1505/1370		
LGTh/RMf	(2920 + 2850)/(2960 + 2870)	Length/Degree of ramification of aliphatic chains: indicator of length versus degree of ramification of aliphatic chains	[35,46]

Afterward, a principal component analysis (PCA) was applied to FTIR bands selected from the second-derivative spectra. The PCA was performed on the correlation matrix using a varimax rotation. This rotation usually leads to clearer patterns and enables the identification of underlying factors influencing peat composition [17]. We also computed multilinear regression (MLR) models for physical (colour) and elemental (C, N, and C/N) peat properties available for core TPD-1. We used stepwise mode to obtain the smallest set of variables needed to fit the data and to avoid redundancy (i.e., collinearity) in the predictors set. We used <1% of the explained variance as a stop criterion for predictor inclusion, i.e., when including a new variable resulted in a <1% increase in the explained variance, the modelling was stopped, and the previous step was selected as the final model.

2.4. Additional Data

As mentioned above, we also used additional data from the TPD-1 core described and discussed in a previous investigation [29]. These include the following: CIELab colour parameters (lightness (L*), the green-red component (a*), the blue-yellow component (b*)), organic elemental data (C %, N %, and C/N), and the inorganic composition (ash content %, Titanium mg kg^{-1}, and Rubidium mg kg^{-1}). The depth records of these properties can be found in the Supplementary Materials (Figure S1). The objective is to support the usefulness of the MIR data (i.e., molecular composition of the peat) to understand changes in physical (i.e., colour) and chemical properties of the peat.

3. Results

3.1. Spectral Signal

The FTIR spectra of the measured peat samples, as well as their average, standard deviation, and average second-derivative spectra are presented in Figure 2. As it is readily apparent, the spectral signals of the analysed samples from the two peat cores (TPD-1 and TPD-2) look very much alike and are indicative of typical FTIR absorbance spectra of peat material. All the spectra have many features in common, such as the broad absorption occurring between 3400 and 3200 cm^{-1}, two well-defined peaks at bands around 2919 and 2850 cm^{-1}, and numerous individual peaks within the fingerprint region between 1800 and 700 cm^{-1}, representative of peat organic matter (pOM) [19,21,47,48].

Some of the most stand-out peaks are presented in Table 2, with their assignments corresponding to the type of chemical bond. The listed absorption bands are characteristics of the molecular structure in polysaccharides (i.e., 3288, 1733, 1031, and 839 cm^{-1}), aliphatics (2919, 2850, 1377, and 721 cm^{-1}), lignin and other aromatic compounds (i.e., 1590, 1510, and 1263 cm^{-1}), and nitrogenated (i.e., proteinaceous) compounds (1657 and 1463 cm^{-1}) [14–16,42]. An overall comparison using the average and standard deviation spectra helps to emphasize the quite similar molecular composition of the two peat cores and to conveniently identify the possible differences between them in relation to a few specific bands (i.e., 3288, 2919, 2850, 1590, 1263, and 1031 cm^{-1}). Furthermore, the average second-derivative spectra enable the resolution of a larger number of individual peaks. These resolved peaks are further investigated through a chemometric FTIR data analysis to shed light on the molecular structure of the two peat cores' organic chemical constituents.

Table 2. Main FTIR absorption bands of TPD-1 and TPD-2 peat samples.

Bands	Assignments	References
3298	hydroxyl (O–H) groups in cellulose, alcohols, phenols and water molecules	[16,47]
2918	Asymmetric stretching of aliphatic C–H in fats, wax, lipids	[14,16,47]
2849	Asymmetric stretching of aliphatic C–H, in fats, wax, lipids	[15,16,47]
1733	C=O stretching of carbonyl functions, particularly aldehydes, ketones, and carboxyl groups; in hemicellulose	[47]
1705	C=O stretch of COOH (free organic acids)	[16]
1681	C=O stretch aromatic ketones	[48]
1653	aromatic C=C vibrations and COO^- groups, C=O of amide I in proteinaceous origin	[15,16,47]
1629	aromatic C=C vibrations and COO^- groups	[15,47]
1593	C=C stretching, lignin	[48]
1543	Secondary amide N–H bending, C–N stretching	[48]
1509	aromatic skeletal vibrations, conjugated C=N systems and amino functionalities, lignin or phenolic backbone	[47]
1461	(amide II) aromatic skeletal vibrations, conjugated C=N systems and amino functionalities, lignin or phenolic backbone	[48]
1420	typically ascribed to O–H deformations of phenolic and aliphatic groups	[47]
1373	typically ascribed to O–H deformations of phenolic and aliphatic groups	[47]
1265	C–O stretching of ethers and/or carboxyl groups, indicative of lignin backbone	[16,47]
1157	C–O stretching of polysaccharide structures, cellulose	[19]
1123	C-O stretching vibrations in polysaccharide, and aromatic C-H deformation vibrations in syringyl units, lignin	[14]
1077	C–O stretching of polysaccharide structures, cellulose	[47]
1030	C–O stretching of polysaccharide structures, cellulose	[47]
987	C–O stretching of polysaccharide structures	[47]
896	O–H, carbohydrates	[28]
833	Aromatic CH out of plane, lignin	[14,16]
719	Aliphatic groups, CH_2 wag	[14,16]

3.2. MIR Indices

The records of the MIR indices are shown in Figure 3, grouped in seven main depth patterns based on their similarities. The first pattern is shown by PS/AL, PS/AR, and CB/AR, indices that are highly correlated (Pearson correlation coefficient r 0.73–0.95, $p < 0.01$; Table S1) between them. They show a rapid decrease in the upper 20 cm of the cores and almost constant or slightly decreasing values with depth. Values do not differ much between TPD-1 and TPD-2 (Figure 3). Apart from the main trend, the CB/AR ratio also shows a secondary pattern of shorter cycles of variation.

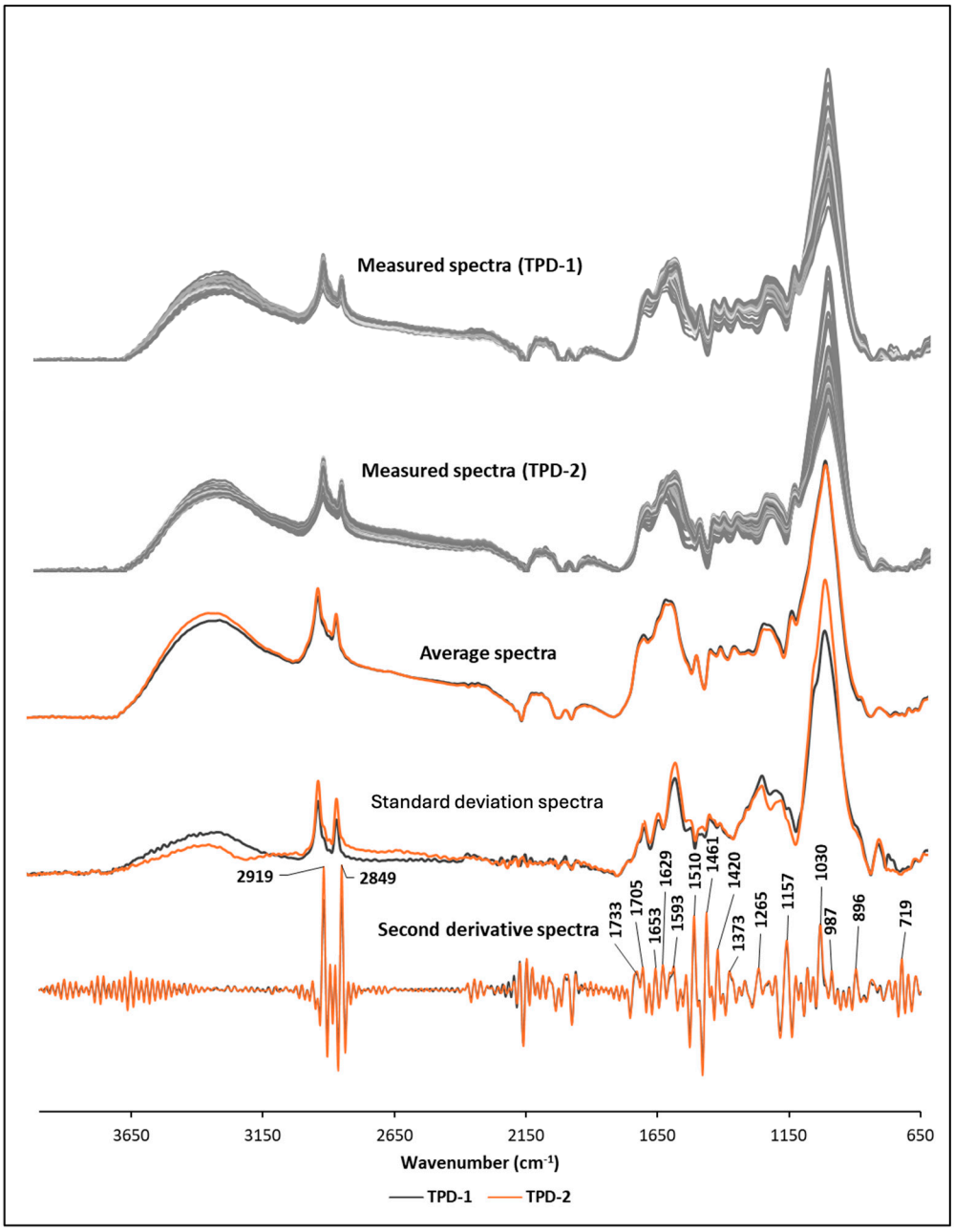

Figure 2. FTIR measured spectra, average spectra, standard deviation spectra, and average second-derivative spectra (values are reversed to match absorbances) of the TPD-1 and TPD-2 peat samples from the Tremoal do Pedrido mire.

AL/AR and CCr-1 show a second pattern of depth variation (r 0.72, $p < 0.019$). The trend shows four main peaks/troughs and no depth dependency (Figure 3). The values for TPD-1 and TPD-2 are quite similar or almost identical for AL/AR, but for CCr-1, TPD-1 has consistently higher values than TPD-2.

LGth/RMf, representing a third depth pattern, shows an overall increase with depth but with some wiggles that are opposite to those of the indices of the second pattern but like those of the secondary variations of CB/AR (Figure 3).

Two of the lignin indices (G/S-1 and G/S-3) share a fourth pattern of depth variation (r 0.68, $p < 0.01$; Table S1), with a sharp sub-superficial peak (5–6 cm), a strong decrease until 13 cm, and values increasing slowly until 56 cm that decrease again until 105 cm (Figure 3). Both cores share the same pattern, although in the lower section, the TPD-1 values do not decrease as apparently as in TPD-2, at least until 80 cm.

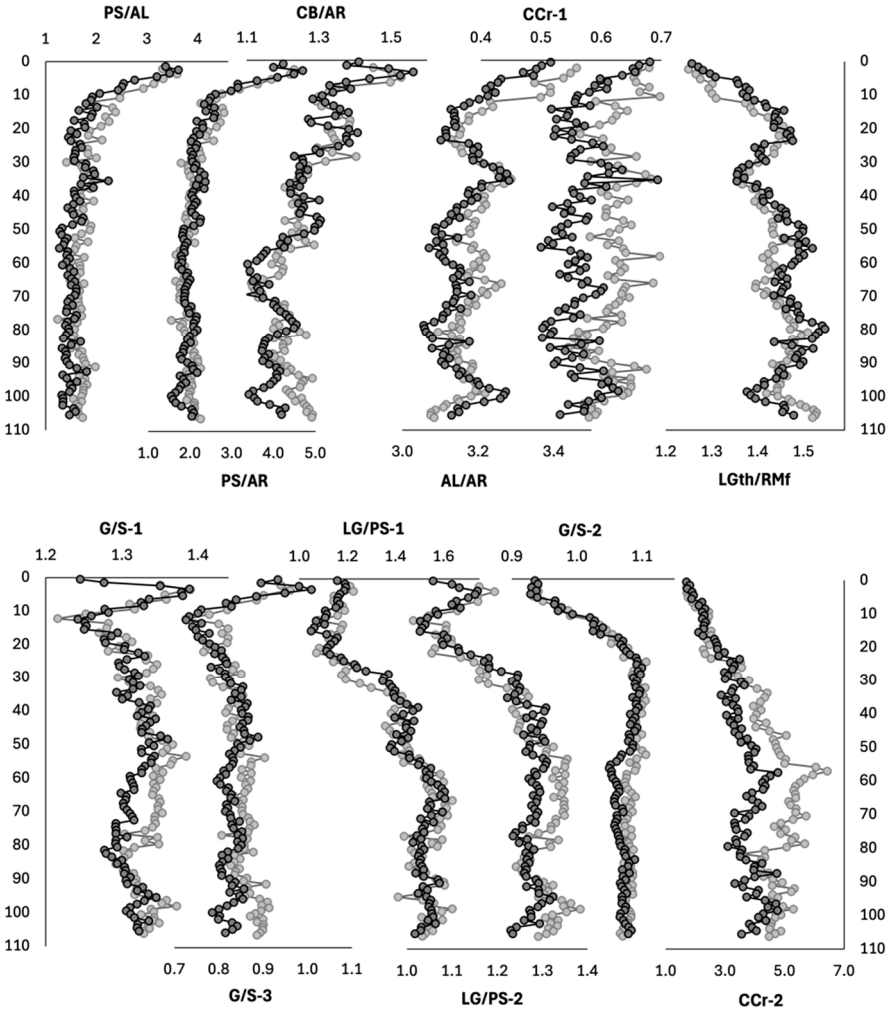

Figure 3. Depth records of the MIR indices. TPD-1, grey line; TPD-2, black line. For the meaning of codes of the MIR indices, see Table 1.

The lignin/polysaccharide indices (LG/PS-1 and LG/PS-2) show a fifth pattern of depth variations (r 0.93, $p < 0.01$; Table S1) (Figure 3). Three main sections can be distinguished: in the upper 22 cm the values are lower, with LG/PS-2 showing a sub-superficial peak (4 cm); from 22 to 30 cm, the values increase abruptly; and below that, the depth values show much smaller variations—although LG/PS-1 values seem to increase in two steps, 30–39 and 54–64 cm. The TPD-1 core values lag behind those of TPD-2 by about 5 cm in the transition section (22–30 cm).

The sixth pattern of depth variation of the G/S-2 index is characterized by low and constat values in the upper 6 cm, a rapid increase with depth until 25 cm, and almost constant values below that depth (Figure 3). Both cores have rather similar values.

The seventh pattern is that of CCr-2, characterized by two step increases, from the top to a depth of 24 cm and from there to a depth of 57 cm, with smaller variations in the section below (Figure 3).

These MIR indices also show negative correlations between them, reflecting opposite trends. The most notable ones are those between the indices of the first depth pattern (PS/AL, PS/AR, and CB/AR) and the third (LGth/RMf), fifth (LG/PS-1, LG/PS-2), sixth (CCr-2), and seventh (G/S-2) patterns of depth changes (Table S1).

3.3. Principal Component Analysis (PCA)

For the PCA, we selected 59 MIR absorbances based on the second-derivative spectra of the samples of the two peat cores (Figure 2). The PCA extracted eight main components that explain 97.4% of the MIR variance, with absorbances' communalities being between 0.92 and 1.00 (i.e., 92 to 100% of the variance of the absorbances are captured by the eight extracted principal components). The first component, Cp1 (43.7% of total MIR variance), is dominated by polysaccharide (i.e., cellulose) absorbances, which have large positive loadings (>0.75), and aromatic (i.e., lignin) and carboxylic absorbances, which have large negative loadings (Table S2). The component reflects a balance between fresh (i.e., polysaccharides) and resistant (i.e., lignin) peat organic matter (pOM). The depth record of the variation in Cp1 scores is quite similar for both cores, TPD-1 and TPD-2, showing a rapid decrease in fresh pOM and an increase in resistant pOM in the upper 20 cm and almost stable scores with depth—with small wiggles (Figure 4).

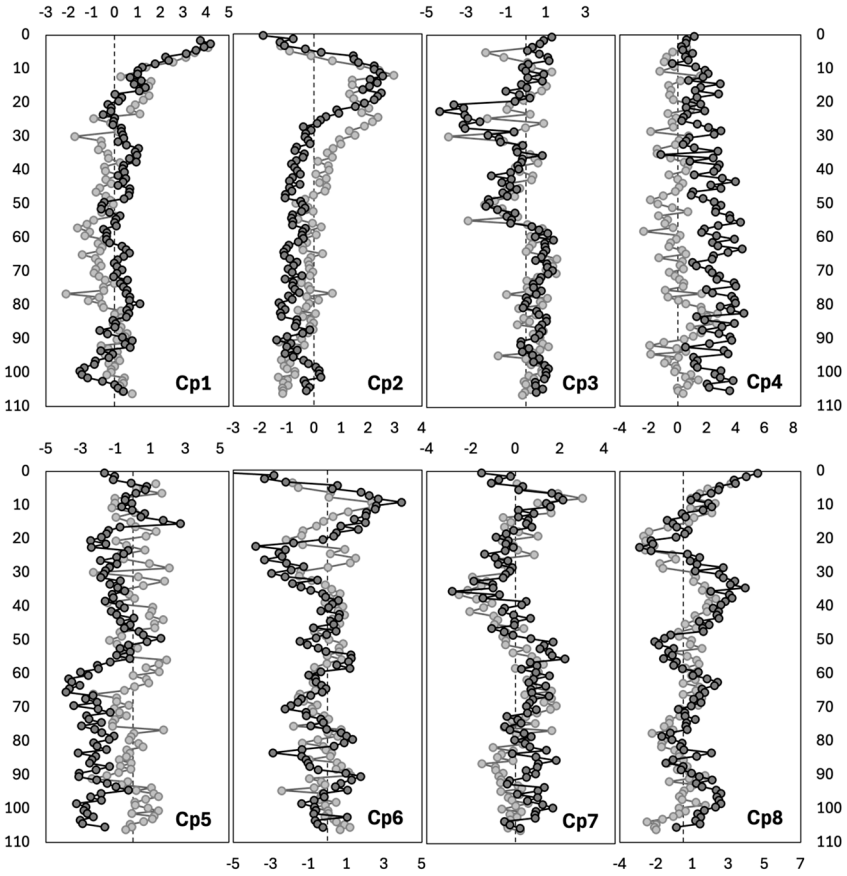

Figure 4. Depth records of the scores of the eight extracted principal components. TPD-1, grey line; TPD-2, black line. The dashed line represents the zero value.

The second component, Cp2 (24.6% of total MIR variance), is dominated by large positive loadings of absorbances of nitrogenated compounds (amide I and amide II vibrations, Table S2) and large negative loadings of absorbances related to lignin. The component reflects a gradient of depletion of nitrogenated pOM compounds versus enrichment in lignin. The record of scores shows a rapid increase with depth until 10 cm, stable values between 10 and 20(25) cm, a rapid decrease until 30–35 cm, and almost stable values to 105 cm (Figure 4). The overall changes are the same for both cores, but TPD-1 seems to lag behind TPD-2 by about 5 cm.

The third component, Cp3 (13.3% of total MIR variance), is related to variations in phenolic and aliphatic (methyl and methylene) absorbances (Table S2). The depth record

of scores shows two negative excursions (i.e., depletion in phenolics and aliphatics), at 20–32 cm and 45–56 cm, with little variation in the rest of the cores. TPD-1 seems to be slightly decoupled from TPD-2 in the uppermost excursion (Figure 4).

The fourth component, Cp4 (8.5% of total MIR variance), is almost exclusively related to variations in the aliphatic absorbances in the 3000–2800 cm^{-1} region (Table S2). The depth records of scores of the two cores show no distinctive pattern, with small variations and a somewhat slight increase in values from the top to 30–35 cm, which is more evident in TPD-2 (Figure 4). In that section, the TPD-1 and TPD-2 scores are quite similar, but below that depth, TPD-1 shows consistently lower scores than TPD-2.

The fifth component, Cp5 (2.6% of total MIR variance), accounts for the variance of two carboxylic absorbances of free organic acids and salts of organic acids (Table S2). Higher Cp5 score values are shown in the upper 56 cm of the TPD-2 core, and much lower negative values are shown below that depth (Figure 4). TPD-1 has a similar depth distribution, but the section of higher scores extends a bit further in depth (63 cm); the decrease in the section below is not as pronounced as in TPD-2, and the values recover below 95 cm.

The sixth component, Cp6 (2.4% of MIR variance), accounts for most of the variation in only one absorbance (Table S2) related to guaiacyl (G) lignin units. The depth records of the scores are quite similar for the two cores, peaking at 10, 44, 59, 80, and 91 cm, with the first peak being the largest (Figure 4). TPD-1 shows an additional peak at 26 cm.

The other two components, Cp7 (1.4% of MIR variance) and Cp8 (1.0% of MIR variance), are related to minor amounts of variance of polysaccharides and aliphatics, respectively (Table S2). TPD-1 and TPD-2 show quite similar depth records of scores (Figure 4). The Cp7 and Cp8 records are largely opposite, with the Cp7 records being similar and the Cp8 records being opposite to that of Cp6.

Regarding the relationship between the extracted components and the MIR indices (Table 3), Cp1 is positively correlated with PS/AR (r 0.93, $p < 0.01$), PS/AL (r 0.83, $p < 0.01$), and CB/AR (r 0.65, $p < 0.01$) and negatively correlated with G/S-2 (r −0.83, $p < 0.01$), CCr-2 (−0.78, $p < 0.01$), LG/PS-1 (−0.53), and LG/PS-2 (−0.50). Cp2 is negatively correlated with LG/PS-1 (r −0.75, $p < 0.01$), LG/PS-2 (r −0.76, $p < 0.01$), and G/S-3 (−0.68). Cp4 is negatively correlated with CCr-1 (r −0.821, $p < 0.01$), and Cp8 is positively correlated with AL/AR (r 0.63, $p < 0.01$) and negatively correlated with LGth/RMf (r −0.67, $p < 0.01$).

Table 3. Correlation (Pearson coefficient) between the principal components and MIR indices. For the meaning of the codes of the MIR indices, see Table 1.

	PS/AR	PS/AL	AL/AR	LGth/RMf	CB/AR	G/S-1	G/S-2	G/S-3	LG/PS-1	LG/PS-2	CCr-1	CCr-2
Cp1	0.93	0.83	0.43	−0.48	0.65	−0.11	−0.80	0.28	−0.50	−0.53	0.09	−0.78
Cp2	0.12	0.14	0.17	−0.28	0.36	−0.40	−0.13	−0.68	−0.75	−0.76	0.06	−0.38
Cp3	0.01	0.10	0.14	−0.05	−0.45	−0.09	−0.21	0.09	0.38	0.14	0.26	0.18
Cp4	−0.20	−0.44	−0.42	0.38	−0.34	−0.38	0.03	−0.34	0.16	0.00	−0.87	−0.25
Cp5	0.19	0.25	0.14	−0.12	0.47	0.29	−0.05	0.23	−0.29	−0.08	0.31	0.06
Cp6	−0.09	−0.12	−0.20	0.21	−0.02	0.00	−0.07	−0.15	−0.01	−0.04	−0.14	0.03
Cp7	−0.13	−0.17	−0.12	0.16	−0.21	0.00	−0.28	−0.20	0.11	0.06	−0.26	0.08
Cp8	0.30	0.35	0.63	−0.67	−0.02	0.00	−0.25	0.13	0.01	−0.02	0.25	−0.20

3.4. Multilinear Regression Analysis (MLR): MIR and Peat Properties

We computed MLR models using as response variables (L*, a*, b*) the peat OM (C, N, and C/N) properties of the TPD-1 core and as predictors the scores of the extracted principal components (Cps). All models showed high correlation coefficients (0.77 to 0.98, Table 4), and four to five Cps were needed to model the response variables. Nitrogen content required the smallest set (four) of predictors. In general, the first three Cps were included in all the models, with the exception of Cp1 for redness (a*), and have the largest regression coefficients.

Table 4. Summary statistics of the multilinear regression models using MIR indices and the PCA extracted components to fit colour (lightness, L*; redness, a*; and yellowness, b*) and peat organic matter composition (C %, N %, and C/N ratio). R, correlation coefficient; error, error of the estimate; and regression coefficients.

	R	Error	Constant	Cp1	Cp2	Cp3	Cp4	Cp6	Cp7	Cp8
L*	0.87	1.9	27.2	2.40	1.56	−1.07	−0.55			0.43
a*	0.77	0.5	7.5		0.32	−0.33	−0.22	0.12	−0.19	
b*	0.89	0.9	15.0	1.00	1.07	−0.91	−0.44	0.37		
C	0.98	0.4	50.7	−1.58	−1.31	0.41	0.10			−0.30
N	0.97	0.1	1.7	0.20	0.29	−0.04		0.06		
C/N	0.98	1.2	31.1	−4.01	−4.60	1.21		−0.86	0.85	

As for the colour parameters, lightness (L*) increases with increasing Cp1, Cp2, and Cp8 values and decreases with increasing Cp3 and Cp4 values. Cp2 and Cp6 have a positive effect and Cp3, Cp4, and Cp7 have a negative effect on redness (a*). Cp1, Cp2, and Cp6 have a positive effect on yellowness (b*) and Cp3 and Cp4 have a negative effect. Overall, the first four components are the ones more largely related to peat colour changes in the TPD cores. The fitting between observed and predicted values is better for L* and b* than for a* (Figure 5).

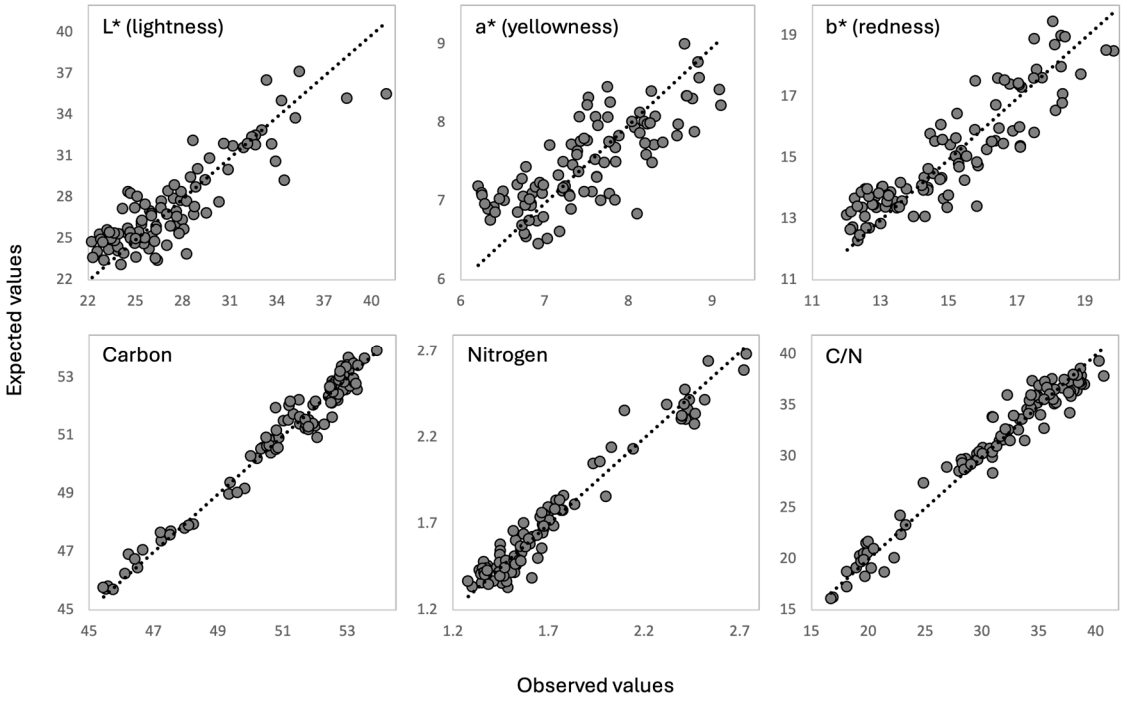

Figure 5. Relationship between observed and expected values, obtained with the multilinear regression models, for the peat properties of the TPD-2 core. L*, a*, b*: CIELab space; C and N in percentage.

The models of the elemental composition (C, N, and C/N) of pOM are the ones with the largest correlation coefficients (Table 4) and, thus, the better fitting between observed and predicted values (Figure 5). Carbon content is negatively related to Cp1, Cp2, and Cp8 and positively related to Cp3 and Cp4. Nitrogen content is positively related to Cp1, Cp2, and Cp6 and negatively related to Cp3. The C/N ratio is positively related to Cp3 and Cp7 and negatively related to Cp1, Cp2, and Cp6.

4. Discussion

4.1. Changes in the Molecular Composition of the Peat

Both the MIR indices and the extracted principal components on selected peaks of the MIR spectra reflect intense depth changes in the molecular composition of the pOM of the studied cores (TPD-1 and TPD-2). The main change in pOM composition is represented by two opposite trends: that of PS/AL, PS/AR, CB/AR, and Cp1, and that of LGth/RMf, LG/PS-1, LG/PS-2, CCr-2, and G/S-2. This implies that as polysaccharides and carbonyl-rich compounds are depleted, the pOM is enriched in lignin, aliphatics, and guaiacyl lignin moieties (versus the syringyl ones), and the length of the aliphatic chains and cellulose crystallinity tend to increase as well. This overall dominant pattern is driven by long-term peat decomposition that produces exponential depletion of labile pOM compounds and results in the accumulation of resistant pOM compounds. These results agree with previous investigations that also found that the decay of polysaccharides was accompanied by the accumulation of lignin and aliphatic compounds [33,47,49–52]. Despite this, lignin showed a more complex evolution than that of aliphatics, in part because they seem to be active in the process of accumulation (i.e., they can inhibit peat decomposition), while the accumulation of the aliphatics is more passive and directly related to the depletion of the more labile organic compounds [53–55].

AL/AR, CCr-1, and Cp8 also show similar depth records, opposite to that of Cp6. CB/AR and LGth/RMf also show these opposite variations, as a secondary trend over-imposed on the variation related to long-term peat decomposition. These represent a series of alternating short-term changes, which typically include four main cycles of higher and lower values. Increases in aliphaticity (AL/AR and Cp8) and cellulose crystallinity (CCr-1) are accompanied by decreases in carbonyl-rich compounds (CB/AR), the length of the aliphatic chains, and guaiacyl lignin moieties (Cp6), and vice versa. These variations may be coupled to short-term variations in bog surface wetness and related oxygen availability in the superficial sections of the peatland, which, in ombrotrophic mires, have been related to variations in rainfall [17].

The G/S indices (G/S-1 and G/S-3) and Cp7 also share a similar depth record: guaiacyl lignin moieties and some polysaccharides show a rapid increase in the upper few centimetres of the peat deposit, followed by a sharp decrease and slower recovery with depth. As found in our study, different lignin functionalities have different susceptibilities to degradation, with syringyl units being more prone to degradation than guaiacyl units [56,57]. In a previous investigation in a boreal peatland, we found that G/S was only partially related to long-term peat decomposition [17]. Thus, changes in G/S certainly reflect both changes in plant communities and in peat decomposition.

Cp2 also shows a depth record characterized by a significant sub-superficial enrichment, followed by a rapid depletion, which involves the opposite depth distribution of bands associated with nitrogenated compounds versus bands associated with lignin vibrations. These two kinds of compounds overlap in the 1700–1500 cm^{-1} region and are sometimes difficult to disentangle. Cp2 scores are highly correlated to the total nitrogen content of the peat for the TPD-1 core (r 0.77, $p < 0.01$), which supports the interpretation of the bands with positive loadings as reflecting nitrogenated compounds. Nitrogen is rapidly recycled in the upper sections of the peat deposit through microbial activity due to the decomposition of plant remains and the assimilation of nitrogen-rich compounds [27,58,59]. This is consistent with the rapid turnover of labile nitrogen pools observed under aerobic conditions [60]. While many peatlands are characterized by slow decomposition rates due to their acidic conditions, the recycling of nitrogen stimulates microbial processes, enhancing the breakdown of organic matter [61].

The other two main changes reflected by the principal components, but not by the MIR indices, are those shown by Cp3 and Cp5. As indicated above, a secondary variation in phenolic and aliphatic compounds (Cp3) is characterized by two negative excursions at a depth of between 20 and 56 cm, while a secondary carboxylic signal (Cp5) shows relatively elevated values in the upper 56 cm and lower values below that depth. As a preliminary hypothesis, we suggest that these patterns may reflect changes in the source of the pOM, i.e., primarily resulting from variations in vegetation composition. Research based on plant macrofossils has shown that plant community changes are closely linked to fluctuations in hydrology and microtopography. These shifts, in turn, influence plant productivity and decomposition rates, ultimately affecting pOM composition [62–64].

Regarding the pOM molecular composition, two final remarks can be made. On one hand, some of the indices related to the same pOM compounds may show almost identical depth variations, while others show quite different depth variations. The first is the case for indices involving compounds affected by long-term peat decomposition, such as PS/AR, PS/AL, LG-PS-1, LG-PS2, and Cp1, which points to decomposition as one of the main factors driving pOM change. The second can be exemplified by the CCr indices: the CCr-1 record seems to respond to short-term decomposition, while CCr-2 seems to be mostly related to long-term peat decomposition. The increasing trend of CCr-2 may be indicative of preferential degradation of the more amorphous phases of the cellulose, producing a relative increase in the more crystalline phases. But plant composition may also influence the molecular structure of the polysaccharide compounds, and this also plays a role in cellulose crystallinity. This can be attributed to the different chemical signatures and diagenetic properties of the mosses compared to vascular plants [65]. At the same time, the microbial community and the decomposition rates of cellulose can influence cellulose crystallinity, as suggested by the changes in the crystallinity indices. In this regard, although specific environmental factors (i.e., the availability of oxygen and nutrients, temperature, etc.) can play a significant role in microbial activity, it has been suggested that the type of vegetation may favour the occurrence of specific cellulolytic microorganisms that direct cellulose degradation [66,67]. Thus, the more complex pattern of CCr-1 and its dependence on short-term changes point to a coupling of enhanced/decreased degradation during dry/wet phases and the concomitant changes in bog vegetation and microbial communities' activity.

On the other hand, the depth variations of some compounds are related to more than one MIR index and principal component, suggesting a more complex range of processes driving their change. This is the case, for example, of lignin, which is affected by long-term variations, short-term variations, and the differential evolution of the guaiacyl and syringyl lignin moieties—possibly coupled to wetness phases.

4.2. Within-Bog Variability

TPD-1 and TPD-2 show quite similar records for the twelve MIR indices, with CCr-1 being the only index with a consistent difference in intensity between cores (at all depths, values for TPD-2 are higher than values from TPD-1). PS/AL, PS/AR, LGth/RMf, and G/S-2 present the highest similarity between the cores. With the exception already mentioned of CCr-1, almost all indices show similar values in the upper section (0–22 cm) of both cores. The section between 22 and 50 cm is also very homogeneous between cores, but in TPD-2 LG/PS-1 and LG/PS-2 TPD-1, the values lag behind those of TPD-2 by about 5 cm in the transition section (22–30 cm). Slight decouples seem to be more common in the section between 50 and 80 cm, where TPD-1 has consistently higher values than TPD-2 for the secondary cycles of CB/AR, AL/AR, LGth/RMf, G/S-1, G/S-3, and LG/PS-2, while in CCr-1, the higher values of TPD-1 start a few centimetres above (from 30 to 80 cm). The

bottom section also seems to be very homogeneous, with the TPD-1 values being slightly higher between 100 and 110 cm for CB/AR, LGth/RMf, G/S-3, and LG/PS-2.

According to our results, cellulose crystallinity (both CCr-1 and CCr-2) shows the highest differences between cores. This may be related to small changes in vegetation composition between cores due to, for example, microtopography (e.g., hummocks vs. hollows) or local differences in microbial activity. In the first case, the crystallinity of cellulose may differ between different bog plants, since differences in crystal size have been detected between algae and higher plants [68,69]. In the second case, the microorganisms may tend to preferentially degrade the more amorphous (or smaller crystal size) components of the cellulose, producing a secondary increase in the more crystalline (or higher crystal size) cellulose (hydrolysis performance decreases with increasing crystallinity, as indicated by [70]). In contrast, the indices traditionally linked to peat decomposition (PS/AL, PS/AR, and LGth/RMf) display the most similar values between cores, suggesting that both cores suffered from comparable and equally intense decomposition processes along depth/time. The slight differences and similarities observed in the peat sections may respond to small differences and similarities in vegetation composition, since small changes in the water table exert a strong control on species abundance [71,72]. In fact, the section from 50 to 80 cm could be linked to a slightly higher abundance of mosses in TPD-1, indicated by the relatively higher content of carboxylic compounds (CB/AR), as well as changes in the amount and type of lignin (G/S-1, G/S-3, and LG/PS-2), since moss tissues and derived soil OM differ in their aromatic and aliphatic signal from other vegetation [73]. However, the "harmony" in the two cores regarding the MIR indices is the most important result.

The eight principal components show a very similar behaviour and intensity between cores, except for Cp4 and Cp5, which maintain similarities but are less pronounced. Scores of Cp4 are quite similar between cores, but below a 35 cm depth, TPD-2 shows consistently higher scores than TPD-1. For Cp5, below 10 cm score values of TPD-1 tend to behave similar with higher values than TPD-2; however, both behave opposite at ~60 cm and in the lowest part (~100 cm). The two cores almost mimic their variation in Cp1, Cp7, and Cp8. For Cp2, TPD-1 seems to lag behind TPD-2 by about 5 cm, most likely due to local differences in peat accumulation; Cp3 variation only shows slight decouples around 10 and 30 cm, respectively, and TPD-1 shows an additional peak at 26 cm in Cp6.

Cp4 and Cp5 are related to aliphatic and carboxylic absorbances, respectively. The observed differences between cores are opposite, since TPD-2 shows a higher intensity for aliphatic bands, while TPD-1 shows a higher intensity for carboxylic ones. This fact agrees with the observed changes between cores in the MIR indices. Since carboxylic compounds can be related to moss abundance compared to grasses [74], or litter and shrubs [75], the slight differences could be due to vegetation (mosses more abundant in TPD-1). But it can also be related to differences in carboxylic microbial degradation between cores [76], especially in the section from 50 to 80 cm. If any of those existed, they seem to have been minor. As happened with the MIR indices, the principal component analysis results remark the similarities between both cores, rather than differences.

4.3. Changes in pOM and Relationship to Peat Properties

To support the information content of the MIR data, we computed MLR models to fit the physical and elemental properties of the pOM of TPD-1 core. All models resulted in good-to-excellent fitting—for the elemental pOM composition in particular (Table 4). The results of these models suggest that the depletion of labile pOM and the accumulation of resistant pOM (Cp1), the depletion in N-compounds and the accumulation of lignin (Cp2), and the depletion of phenolic and aliphatic pOM (Cp3) are the main drivers of colour and elemental compositional (C, N, and C/N) change. These changes are essentially related to

long-term peat decomposition: as decomposition progresses, the peak becomes darker and redder, N is depleted, and C and C/N increase. The intensity of change is higher in the upper 25–30 cm of the cores, which could be related to more intense aerobic decomposition at the superficial section due to higher oxygen availability.

As for the secondary MIR signals (Cp4 to Cp8), related to shorter-term variations, the specific variation in aliphatic pOM (Cp4) is significantly related to changes in peat colour, but its weight on the elemental composition of the pOM (C, N, and C/N) is low or negligible. The other molecular MIR components have low-to-moderate effects on some colour parameters and elemental properties, but Cp5 was not loaded in any of the models. In a previous modelling exercise of peat properties of a long (9000 years) record of a boreal peatland, we obtained quite similar results. MIR data were highly efficient in modelling peat C, N, and C/N [59].

5. Conclusions

The present study provides evidence of the homogeneity in pOM composition, at a short distance (~30 m), within the dome of a single ombrotrophic mire. The two analysed cores from Tremoal do Pedrido show very similar behaviour and intensity of changes with depth. This "harmony" is attested even in those compounds that show intense variations with depth. Indeed, MIR indices and the principal components exhibit profound changes in the molecular composition of the pOM of the studied cores. A combination of long-term decomposition processes and short-term modifications of the hydrology of the dome seems to have driven the main changes in pOM. Changes in vegetation and microbial activity may have also played a role on the accumulation of phenolic, aliphatic, and nitrogenated compounds, respectively.

Spectroscopic techniques used to address peat variability have shown to be useful in detecting changes in organic matter compound variation. The statistical approach that combines MIR indices with the PCA obtained from second-derivative selected bands complement each other. This combination of approaches is especially effective when dealing with compound distributions that are affected by more than one process, such as long- and short-term variations (e.g., lignin). While most indices show large similarities between cores, cellulose crystallinity shows within-bog differences. Crystallinity indices are commonly used in plant and wood research and, to our knowledge, are applied here for the first time to investigate the molecular composition of pOM. Our study opens an interesting question as to whether crystallinity variations are related to the source vegetation or to microbial activity, or a combination of both, at the surface of the peatland or at depth in the peat deposit.

Finally, the query of whether properties within a single peatland are maintained at depth in different locations has been taken a step forward by our study, showing that they appear to be maintained for ombrotrophic peatlands, or at least in this case study. More research in other ombrotrophic peatlands, such blanket bogs, and minerotrophic peatlands, such as fens, will be needed in order to explore in depth the spatio-temporal responses of the pOM molecular composition. For the Tremoal do Pedrido dome, the two cores researched by us sang a two-part harmony song during the last 1400 years, most of the time with the same pitch.

Supplementary Materials: The following supporting information can be downloaded at https://www.mdpi.com/article/10.3390/soilsystems9010014/s1, Figure S1: Depth records of the TPD-1 core peat properties used in the modelling exercise; Table S1: Correlation (Pearson coefficient) between MIR indices; Table S2: Loadings of the selected absorbances for the eight extracted principal components; file FTIR-TPD.xlsx: standardized absorbance values of the selected bands used in the principal components analysis.

Author Contributions: Conceptualization, A.M.C. and M.T.; methodology, A.M.C., M.T. and A.F.G.; formal analysis, A.M.C., A.F.G., M.T. and O.L.-C.; investigation, A.M.C., A.F.G., M.T. and O.L.-C.; resources, A.M.C. and O.L.-C.; data curation, A.F.G.; writing—original draft preparation, A.M.C., A.F.G., M.T. and O.L.-C.; writing—review and editing, A.M.C., A.F.G., M.T. and O.L.-C.; visualization, A.M.C., A.F.G., M.T. and O.L.-C.; funding acquisition, A.M.C. and O.L.-C. All authors have read and agreed to the published version of the manuscript.

Funding: This research was funded by the Grupos de Referencia Competitiva (ED431C 2021/32, Xunta de Galicia) and European Union (ERC Consolidator Grant, PollutedPast, 101087832). The views and opinions expressed are, however, those of the author(s) only and do not necessarily reflect those of the European Union or the European Research Council. Neither the European Union nor the granting authority can be held responsible for them. The OLC is funded by Ramón y Cajal 2020 (RYC2020-030531-I).

Institutional Review Board Statement: Not applicable.

Informed Consent Statement: Not applicable.

Data Availability Statement: The data presented in this study are available as Supplementary Materials.

Acknowledgments: We want to thank Noemí Silva Sánchez and Marta Pérez Rodríguez for helping in field sampling and sampling preparation in the lab.

Conflicts of Interest: The authors declare no conflicts of interest.

References

1. Gorham, E. Northern peatlands: Role in the carbon cycle and probable responses to climate change. *Ecol. Appl.* **1991**, *1*, 182–195. [CrossRef] [PubMed]
2. Limpens, J.; Berendse, F.; Blodau, C.; Canadell, J.G.; Freeman, C.; Holden, J.; Schaepman-Strub, G. Peatlands and the carbon cycle: From local processes to global implications–a synthesis. *Biogeosciences* **2008**, *5*, 1475–1491. [CrossRef]
3. Harenda, K.; Lamentowicz, M.; Samson, M.; Chojnicki, B. The Role of Peatlands and Their Carbon Storage Function in the Context of Climate Change. In *Interdisciplinary Approaches for Sustainable Development Goals*; Springer: Berlin/Heidelberg, Germany, 2018. [CrossRef]
4. Mauquoy, D.; Engelkes, T.; Groot, M.H.M.; Markesteijn, F.; Oudejans, M.G.; Van Der Plicht, J.; Van Geel, B. High-resolution records of late-Holocene climate change and carbon accumulation in two north-west European ombrotrophic peat bogs. *Palaeogeogr. Palaeoclimatol. Palaeoecol.* **2002**, *186*, 275–310. [CrossRef]
5. Wieder, R.K.; Turetsky, M.R.; Vile, M.A. Peat as an archive of atmospheric, climatic and environmental conditions. In *The Wetlands Handbook*; Wiley-Blackwell: Hoboken, NJ, USA, 2009; pp. 96–112.
6. Chambers, F.M.; Booth, R.K.; De Vleeschouwer, F.; Lamentowicz, M.; Le Roux, G.; Mauquoy, D.; Van Geel, B. Development and refinement of proxy-climate indicators from peats. *Quat. Int.* **2012**, *268*, 21–33. [CrossRef]
7. Martinez Cortizas, A.; Pontevedra-Pombal, X.; Garcia-Rodeja, E.; Novoa-Munoz, J.C.; Shotyk, W. Mercury in a Spanish peat bog: Archive of climate change and atmospheric metal deposition. *Science* **1999**, *284*, 939–942. [CrossRef] [PubMed]
8. Bindler, R. Contaminated lead environments of man: Reviewing the lead isotopic evidence in sediments, peat, and soils for the temporal and spatial patterns of atmospheric lead pollution in Sweden. *Environ. Geochem. Health* **2011**, *33*, 311–329. [CrossRef]
9. López-Merino, L.; Martínez Cortizas, A.; Reher, G.S.; López-Sáez, J.A.; Mighall, T.M.; Bindler, R. Reconstructing the impact of human activities in a NW Iberian Roman mining landscape for the last 2500 years. *J. Archaeol. Sci.* **2014**, *50*, 208–218. [CrossRef]
10. Joosten, H.; Couwenberg, J. Peatlands and carbon. In *Assessment on Peatlands, Biodiversity and Climate Change*; Global Environment Centre: Kuala Lumpur, Malaysia; Wetlands International: Wageningen, The Netherlands, 2008; pp. 99–117.
11. Clymo, R.S. The ecology of peatlands. *Sci. Prog.* **1987**, *1933*, 593–614.
12. Delicato, D. Physical-chemical properties and sorption characteristics of peat. Ph.D. Thesis, Dublin City University, Dublin, Ireland, 1996.
13. Sjöström, J.K.; Bindler, R.; Granberg, T.; Kylander, M.E. Procedure for organic matter removal from peat samples for XRD mineral analysis. *Wetlands* **2019**, *39*, 473–481. [CrossRef]
14. Smieja-Król, B.; Fiałkiewicz-Kozieł, B. Quantitative determination of minerals and anthropogenic particles in some Polish peat occurrences using a novel SEM point-counting method. *Environ. Monit. Assess.* **2014**, *186*, 2573–2587. [CrossRef] [PubMed]

15. Hansson, S.V.; Rydberg, J.; Kylander, M.; Gallagher, K.; Bindler, R. Evaluating paleoproxies for peat decomposition and their relationship to peat geochemistry. *Holocene* **2013**, *23*, 1666–1671. [CrossRef]
16. Jong, R.D.; Björck, S.; Björkman, L.; Clemmensen, L.B. Storminess variation during the last 6500 years as reconstructed from an ombrotrophic peat bog in Halland, southwest Sweden. *J. Quat. Sci.* **2006**, *21*, 905–919. [CrossRef]
17. Martínez Cortizas, A.; Sjöström, J.K.; Ryberg, E.E.; Kylander, M.E.; Kaal, J.; López-Costas, O.; Álvarez Fernández, N.; Blinder, R. 9000 years of changes in peat organic matter composition in Store Mosse (Sweden) traced using FTIR-ATR. *Boreas* **2021**, *50*, 1161–1178. [CrossRef]
18. Chapman, S.J.; Campbell, C.D.; Fraser, A.R.; Puri, G. FTIR spectroscopy of peat in and bordering Scots pine woodland: Relationship with chemical and biological properties. *Soil Biol. Biochem.* **2001**, *33*, 1193–1200. [CrossRef]
19. Artz, R.R.; Chapman, S.J.; Robertson, A.J.; Potts, J.M.; Laggoun-Défarge, F.; Gogo, S.; Francez, A.J. FTIR spectroscopy can be used as a screening tool for organic matter quality in regenerating cutover peatlands. *Soil Biol. Biochem.* **2008**, *40*, 515–527. [CrossRef]
20. Martínez Cortizas, A.; López-Merino, L.; Silva-Sánchez, N.; Sjöström, J.K.; Kylander, M.E. Investigating the mineral composition of peat by combining FTIR-ATR and multivariate analysis. *Minerals* **2021**, *11*, 1084. [CrossRef]
21. Zaccone, C.; Rein, G.; D'Orazio, V.; Hadden, R.M.; Belcher, C.M.; Miano, T.M. Smouldering fire signatures in peat and their implications for palaeoenvironmental reconstructions. *Geochim. Et Cosmochim. Acta* **2014**, *137*, 134–146. [CrossRef]
22. Pérez-Rodríguez, M.; Horák-Terra, I.; Rodríguez-Lado, L.; Cortizas, A.M. Modelling mercury accumulation in minerogenic peat combining FTIR-ATR spectroscopy and partial least squares (PLS). *Spectrochim. Acta Part A: Mol. Biomol. Spectrosc.* **2016**, *168*, 65–72. [CrossRef] [PubMed]
23. Bindler, R.; Klarqvist, M.; Klaminder, J.; Förster, J. Does within-bog spatial variability of mercury and lead constrain reconstructions of absolute deposition rates from single peat records? The example of Store Mosse, Sweden. *Glob. Biogeochem. Cycles* **2004**, *18*. [CrossRef]
24. Olid, C.; Garcia-Orellana, J.; Martínez-Cortizas, A.; Masqué, P.; Peiteado-Varela, E.; Sanchez-Cabeza, J.A. Multiple site study of recent atmospheric metal (Pb, Zn and Cu) deposition in the NW Iberian Peninsula using peat cores. *Sci. Total Environ.* **2010**, *408*, 5540–5549. [CrossRef]
25. Van Bellen, S.; Dallaire, P.L.; Garneau, M.; Bergeron, Y. Quantifying spatial and temporal Holocene carbon accumulation in ombrotrophic peatlands of the Eastmain region, Quebec, Canada. *Glob. Biogeochem. Cycles* **2011**, *25*, GB2016. [CrossRef]
26. Loisel, J.; Yu, Z.; Beilman, D.W.; Camill, P.; Alm, J.; Amesbury, M.J.; Zhou, W. A database and synthesis of northern peatland soil properties and Holocene carbon and nitrogen accumulation. *Holocene* **2014**, *24*, 1028–1042. [CrossRef]
27. Pérez-Rodríguez, M.; Cortizas, A.M. Preliminary characterization of microbial functional diversity using sole-C-source utilization profiles in Tremoal do Pedrido mire (Galicia, NW Spain). *Span. J. Soil Sci.* **2014**, *4*, 158. [CrossRef]
28. Martínez Cortizas, A.; Pérez Alberti, A. *Atlas Climático De Galicia*; Xunta de Galicia: Santiago de Compostela, Spain, 1999.
29. Martínez Cortizas, A.M.; López-Costas, O.; Orme, L.; Mighall, T.; Kylander, M.E.; Bindler, R.; Sala, Á.G. Holocene atmospheric dust deposition in NW Spain. *Holocene* **2020**, *30*, 507–518. [CrossRef]
30. Demšar, J.; Curk, T.; Erjavec, A.; Gorup, C.; Hocevar, T.; Milutinovic, M.; Možina, M.; Polajnar, M.; Toplak, M.; Staric, A. Orange: Data Mining Toolbox in Python. *J. Mach. Learn. Res.* **2013**, *14*, 2349–2353.
31. Toplak, M.; Birarda, G.; Read, S.; Sandt, C.; Rosendahl, S.M.; Vaccari, L.; Borondics, F. Infrared orange: Connecting hyperspectral data with machine learning. *Synchrotron Radiat. News* **2017**, *30*, 40–45. [CrossRef]
32. Broder, T.; Blodau, C.; Biester, H.; Knorr, K.H. Peat decomposition records in three pristine ombrotrophic bogs in southern Patagonia. *Biogeosciences* **2012**, *9*, 1479–1491. [CrossRef]
33. Biester, H.; Knorr, K.-H.; Schellekens, J.; Basler, A.; Hermanns, Y.-M. Comparison of different methods to determine the degree of peat decomposition in peat bogs. *Biogeosciences* **2014**, *11*, 2691–2707. [CrossRef]
34. Hodgkins, S.B.; Tfaily, M.M.; McCalley, C.K.; Logan, T.A.; Crill, P.M.; Saleska, S.R.; Rich, V.I.; Chanton, J.P. Changes in peat chemistry associated with permafrost thaw increase greenhouse gas production. *Proc. Natl. Acad. Sci. USA* **2014**, *111*, 5819–5824. [CrossRef]
35. Yao, S.; Cao, J.; Zhang, K.; Jiao, K.; Ding, H.; Hu, W. Artificial bacterial degradation and hydrous pyrolysis of suberin: Implications for hydrocarbon generation of suberine. *Org. Geochem.* **2012**, *47*, 22–33. [CrossRef]
36. Nelson, M.L.; O'Connor, R.T. Relation of certain infrared bands to cellulose crystallinity and crystal lattice type. Part II. A new infrared ratio for estimation of crystallinity in celluloses I and II. *J. Appl. Polym. Sci.* **1964**, *8*, 1325–1341. [CrossRef]
37. Carrillo, F.; Colom, X.; Sunol, J.J.; Saurina, J. Structural FTIR analysis and thermal characterisation of lyocell and viscose-type fibres. *Eur. Polym. J.* **2004**, *40*, 2229–2234. [CrossRef]
38. Poletto, M.; Ornaghi Junior, H.L.; Zattera, A.J. Native cellulose: Structure, characterization and thermal properties. *Materials* **2014**, *7*, 6105–6119. [CrossRef] [PubMed]
39. Lourenço, A.; Araújo, S.; Gominho, J.; Evtuguin, D. Cellulose structural changes during mild torrefaction of Eucalyptus wood. *Polymers* **2020**, *12*, 2831. [CrossRef]

40. Pandey, K.K. A study of chemical structure of soft and hardwood and wood polymers by FTIR spectroscopy. *J. Appl. Polym. Sci.* **1999**, *71*, 1969–1975. [CrossRef]
41. Colom, X.; Carrillo, F.; Nogués, F.; Garriga, P. Structural analysis of photodegraded wood by means of FTIR spectroscopy. *Polym. Degrad. Stab.* **2003**, *80*, 543–549. [CrossRef]
42. Colom, X.; Carrillo, F. Comparative study of wood samples of the northern area of Catalonia by FTIR. *J. Wood Chem. Technol.* **2005**, *25*, 1–11. [CrossRef]
43. Rana, R.; Langenfeld-Heyser, R.; Finkeldey, R.; Polle, A. FTIR spectroscopy, chemical and histochemical characterisation of wood and lignin of five tropical timber wood species of the family of *Dipterocarpaceae*. *Wood Sci. Technol.* **2010**, *44*, 225–242. [CrossRef]
44. Pandey, K.K. A note on the influence of extractives on the photo-discoloration and photo-degradation of wood. *Polym. Degrad. Stab.* **2005**, *87*, 375–379. [CrossRef]
45. Popescu, C.M.; Singurel, G.; Popescu, M.C.; Vasile, C.; Argyropoulos, D.S.; Willför, S. Vibrational spectroscopy and X-ray diffraction methods to establish the differences between hardwood and softwood. *Carbohydr. Polym.* **2009**, *77*, 851–857. [CrossRef]
46. Matrajt, G.; Muñoz Carro, G.M.; Dartois, E.; d'Hendecourt, L.; Deboffle, D.; Borg, J. FTIR analysis of the organics in IDPs: Comparison with the IR spectra of the diffuse interstellar medium. *Astron. Astrophys.* **2005**, *433*, 979–995. [CrossRef]
47. Cocozza, C.; D'Orazio, V.; Miano, T.M.; Shotyk, W. Characterization of solid and aqueous phases of a peat bog profile using molecular fluorescence spectroscopy, ESR and FT-IR, and comparison with physical properties. *Org. Geochem.* **2003**, *34*, 49–60. [CrossRef]
48. Stuart, B.H. *Infrared Spectroscopy: Fundamentals and Applications*; John Wiley Sons: Hoboken, NJ, USA, 2004.
49. Zaccone, C.; Sanei, H.; Outridge, P.M.; Miano, T.M. Studying the humification degree and evolution of peat down a Holocene bog profile (Inuvik, NW Canada): A petrological and chemical perspective. *Org. Geochem.* **2011**, *42*, 399–408. [CrossRef]
50. Silamikele, I.; Nikodemus, O.; Kalnina, L.; Purnalis, O.; Sire, J. *Properties of Peat in Ombrotrophic Bogs Depending on the Humification Process*; Klavins, M., Ed.; Mires and Peat; University of Latvia Press: Riga, Latvia, 2012; pp. 71–95.
51. Kuhry, P.; Vitt, D.H. Fossil carbon/nitrogen ratios as a measure of peat decomposition. *Ecology* **1996**, *77*, 271–275. [CrossRef]
52. Hodgkins, S.B.; Richardson, C.J.; Dommain, R.; Wang, H.; Glaser, P.H.; Verbeke, B.; Winkler, B.R.; Cobb, A.R.; Rich, V.I.; Missilmani, M. Tropical peatland carbon storage linked to global latitudinal trends in peat recalcitrance. *Nat. Commun.* **2018**, *9*, 3640. [CrossRef]
53. Buurman, P.; Nierop, K.G.J.; Pontevedra-Pombal, X.; Martiínez Cortizas, A. Molecular chemistry by pyrolysis–GC/MS of selected samples of the Penido Vello peat deposit, Galicia, NW Spain. In *Developments in Earth Surface Processes*; Martini, I.P., Martínez Cortizas, A., Chesworth, W., Eds.; Elsevier: Amsterdam, The Netherlands, 2006; Chapter 10; Volume 9, pp. 217–240.
54. Kaal, J.; Baldock, J.A.; Buurman, P.; Nierop, K.G.J.; Pontevedra-Pombal, X.; Martínez-Cortizas, A. Evaluating pyrolysis–GC/MS and 13C CPMAS NMR in conjunction with a molecular mixing model of the Penido Vello peat deposit, NW Spain. *Org. Geochem.* **2007**, *38*, 1097–1111. [CrossRef]
55. Bader, C.; Müller, M.; Schulin, R.; Leifeld, J. Peat decomposability in managed organic soils in relation to land-use, organic matter composition and temperature. *Biogeosci. Discuss.* **2017**, *15*, 703–719. [CrossRef]
56. Schellekens, J.; Bindler, R.; Martínez-Cortizas, A.; McClymont, E.L.; Abbott, G.D.; Biester, H.; Pontevedra-Pombal, X.; Buurman, P. Preferential degradation of polyphenols from Sphagnum–4-Isopropenylphenol as a proxy for past hydrological conditions in Sphagnum-dominated peat. *Geochim. Et Cosmochim. Acta* **2015**, *150*, 74–89. [CrossRef]
57. Li, M.; Pu, Y.; Ragauskas, A.J. Current understanding of the correlation of lignin structure with biomass recalcitrance. *Front. Chem.* **2016**, *4*, 45. [CrossRef] [PubMed]
58. Limpens, J.; Heijmans, M.M.; Berendse, F. The nitrogen cycle in boreal peatlands. In *Boreal Peatland Ecosystems*; Springer: Berlin/Heidelberg, Germany, 2006; pp. 195–230.
59. Martínez Cortizas, A.; Traoré, M.; López-Costas, O.; Sjöström, J.K.; Kylander, M.E. Beyond the obvious: Exploring peat vibrationa spectrscopy (FTIR-ATR) data sunig principal components analysis on trasnposed data matrix (tPCA), Store Mosee bog (Sweden). In *Frontier Studies in Soil Science*; Núñez-Delgado, A., Ed.; Springer: Berlin/Heidelberg, Germany, 2024; pp. 217–247.
60. Bridgham, S.D.; Updegraff, K.; Pastor, J. Carbon, Nitrogen, and Phosphorus Mineralization in Northern Wetlands. *Ecology* **1998**, *79*, 1545–1561. [CrossRef]
61. Pankratov, T.A.; Ivanova, A.O.; Dedysh, S.N.; Liesack, W. Bacterial populations and environmental factors controlling cellulose degradation in an acidic Sphagnum peat. *Environ. Microbiol.* **2011**, *13*, 1800–1814. [CrossRef] [PubMed]
62. Castro, D.; Souto, M.; Garcia-Rodeja, E.; Pontevedra-Pombal, X.; Fraga, M.I. Climate change records between the mid-and late Holocene in a peat bog from Serra do Xistral (SW Europe) using plant macrofossils and peat humification analyses. *Palaeogeogr. Palaeoclimatol. Palaeoecol.* **2015**, *420*, 82–95. [CrossRef]
63. Castro, D.; Souto, M.; Fraga, M.I.; García-Rodeja, E.; Pérez-Díaz, S.; Sáez, J.A.L.; Pontevedra-Pombal, X. High-resolution patterns of palaeoenvironmental changes during the Little Ice Age and the Medieval Climate Anomaly in the northwestern Iberian Peninsula. *Geosci. Front.* **2020**, *11*, 1461–1475. [CrossRef]

64. Ryberg, E.E.; Väliranta, M.; Martinez-Cortizas, A.; Ehrlén, J.; Sjöström, J.K.; Kylander, M.E. Postglacial peatland vegetation succession in Store Mosse bog, south-central Sweden: An exploration of factors driving species change. *Boreas* **2022**, *51*, 651–666. [CrossRef]
65. Kuder, T.; Kruge, M.A. Carbon dynamics in peat bogs: Insights from substrate macromolecular chemistry. *Glob. Biogeochem. Cycles* **2001**, *15*, 721–727. [CrossRef]
66. Hiroki, M.; Watanabe, M.M. Microbial community and rate of cellulose decomposition in peat soils in a mire. *Soil Sci. Plant Nutr.* **1996**, *42*, 893–903. [CrossRef]
67. Repečkienė, J.; Jukonienė, I.; Salina, O. Cellulose-decomposing fungi in peatlands occupied by invasive moss *Campylopus introflexus*. *Bot. Lith.* **2012**, *18*, 46–57. [CrossRef]
68. Šturcová, A.; His, I.; Apperley, D.C.; Sugiyama, J.; Jarvis, M.C. Structural details of crystalline cellulose from higher plants. *Biomacromolecules* **2004**, *5*, 1333–1339. [CrossRef] [PubMed]
69. Thygesen, A.; Oddershede, J.; Lilholt, H.; Thomsen, A.B.; Ståhl, K. On the determination of crystallinity and cellulose content in plant fibres. *Cellulose* **2005**, *12*, 563–576. [CrossRef]
70. Li, L.; Zhou, W.; Wu, H.; Yu, Y.; Liu, F.; Zhu, D. Relationship between crystallinity index and enzymatic hydrolysis performance of celluloses separated from aquatic and terrestrial plant materials. *BioResources* **2014**, *9*, 3993–4005. [CrossRef]
71. Nordbakken, J.F. Plant niches along the water–table gradient on an ombrotrophic mire expanse. *Ecography* **1996**, *19*, 114–121. [CrossRef]
72. Bubier, J.L.; Moore, T.R.; Crosby, G. Fine-scale vegetation distribution in a cool temperate peatland. *Botany* **2006**, *84*, 910–923. [CrossRef]
73. Nierop, K.G.; van Lagen, B.; Buurman, P. Composition of plant tissues and soil organic matter in the first stages of a vegetation succession. *Geoderma* **2001**, *100*, 1–24. [CrossRef]
74. Serebrennikova, O.V.; Strel'nikova, E.B.; Russkikh, I.V.; Duchko, M.A. Composition of the lipids of the sphagnum and cotton grass peats in the forest steppe and southern and middle taigas of West Siberia. *Solid Fuel Chem.* **2017**, *51*, 195–204. [CrossRef]
75. Shamrikova, E.V.; Kubik, O.S.; Punegov, V.V.; Gruzdev, I.V. Effect of the biota diversity on the composition of low-molecular-weight water-soluble organic compounds in southern tundra soils. *Eurasian Soil Sci.* **2014**, *47*, 173–181. [CrossRef]
76. Fisk, M.C.; Ruether, K.F.; Yavitt, J.B. Microbial activity and functional composition among northern peatland ecosystems. *Soil Biol. Biochem.* **2003**, *35*, 591–602. [CrossRef]

Disclaimer/Publisher's Note: The statements, opinions and data contained in all publications are solely those of the individual author(s) and contributor(s) and not of MDPI and/or the editor(s). MDPI and/or the editor(s) disclaim responsibility for any injury to people or property resulting from any ideas, methods, instructions or products referred to in the content.